Are all Frames Equal? Active Sparse Labeling for Video Action Detection

Aayush J Rana
aayushjr@knights.ucf.edu

Yogesh S Rawat
yogesh@crcv.ucf.edu

Center for Research in Computer Vision (CRCV)
University of Central Florida

Abstract

Video action detection requires annotations at every frame, which drastically increases the labeling cost. In this work, we focus on efficient labeling of videos for action detection to minimize this cost. We propose ***active sparse labeling (ASL)***, a novel active learning strategy for video action detection. Sparse labeling will reduce the annotation cost but poses two main challenges; 1) how to estimate the utility of annotating a ***single frame*** for action detection as detection is performed at video level?, and 2) how these ***sparse labels*** can be used for action detection which require annotations on all the frames? This work attempts to address these challenges within a simple active learning framework. For the first challenge, we propose a novel frame-level *scoring mechanism* aimed at selecting most informative frames in a video. Next, we introduce a novel *loss formulation* which enables training of action detection model with these sparsely selected frames. We evaluate the proposed approach on two different action detection benchmark datasets, UCF-101-24 and J-HMDB-21, and observed that active sparse labeling can be very effective in saving annotation costs. We demonstrate that the proposed approach performs better than random selection, outperforming all other baselines, with performance comparable to supervised approach using merely 10% annotations. Project details available at https://www.crcv.ucf.edu/research/projects/active-sparse-labeling-for-video-action-detection/

1 Introduction

Video action detection is a challenging problem with lot of applications in security [1, 2], autonomous driving [3, 4] and robotics [5, 6]. It requires spatio-temporal localization of an action in a video. This has led to innovative methods [7, 8, 9, 10, 11, 12] in recent years which rely on annotation on every frame of a video sample, which can be either bounding box [13] or pixel-wise [14]. This is different from action classification where a class label for each video is sufficient for training [15]. Therefore, it is challenging and costly to annotate an action detection dataset at a large-scale and existing datasets are much smaller in size [13, 14] as compared with classification datasets [15, 16, 17, 18, 19].

In this work, we focus on reducing the annotation effort for video action detection. The existing work in label efficient learning for action detection is mostly focused on semi-supervised [20, 21] or weakly-supervised approaches [22, 23, 24, 25]. These methods rely on either video-level annotations [25, 24], point annotations [21], pseudo-labels [20], or reduced bounding-box annotations [26] to reduce labeling effort. They rely on separate (often external) actor detectors and tube linking methods coupled with weakly-supervised multiple instance learning or pseudo-annotations, limiting the practical simplicity for general use. The video-level and pseudo-label approaches trade performance for saving annotations while the point and reduced bounding-box approach still have to annotate each instance to improve the performance. We argue that a lack of selection criteria for annotating only

36th Conference on Neural Information Processing Systems (NeurIPS 2022).

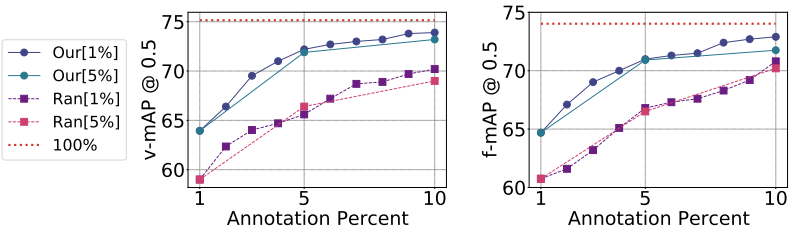

Figure 1: Comparison of our method with different annotation percent and step size against random selection method and fully-supervised method (100% annotations) on UCF-101. Results for 1% and 5% increment at 1%, 5%, and 10% annotations are shown for our and random selection [Ran].

informative data is one of the limitations in these methods. Motivated by this, we propose *active sparse labeling (ASL)* which bridges this gap between high performance and low annotation cost. *ASL* performs partial instance annotation (*sparse labeling*) by frame level selection where the goal is to annotate most informative frames, which are expected to be useful for activity detection task.

Sparse labeling will address the issue of high annotation cost, but there will be some challenges. It will require a frame level cost estimation which can determine the utility of each frame in a video. This estimation should be based on the frame's impact on action detection. Also, the traditional action detection methods require annotations on all the frames [8, 9, 10], therefore existing objective functions will not be effective with sparse labels. We propose a novel uncertainty based frame scoring mechanism for videos, termed as *Adaptive Proximity-aware Uncertainty (APU)*. APU estimates the frame's utility using the uncertainty of the detections and its proximity from existing annotations, determining *diverse* set of *informative* frames in a video which are more effective for learning the task of action detection. In addition, we propose a simple yet effective loss formulation, *Max-Gaussian Weighted Loss (MGW-Loss)*, which uses weighted pseudo-labeling for effective learning from *sparse labels*. Together, the proposed cost estimation algorithm based on APU and the MGW-Loss function helps in reducing the annotation cost while improving model performance at the same time.

We make the following contributions; 1) We propose ***active sparse labeling (ASL)***, a novel active learning (AL) strategy for action detection where each instance is partially annotated to reduce the labeling cost. This is the ***first work*** focused on AL for video action detection to best of our knowledge, 2) We propose a ***novel scoring mechanism*** for selecting *informative* and *diverse* set of frames, 3) We also propose a ***novel training objective*** which helps in effectively learning from *sparse labels*.

We demonstrate the effectiveness of the proposed approach in optimizing annotation cost for video action detection in two different datasets, UCF-101-24 and J-HMDB-21. We reduce the annotation cost by $\sim$ **90%** with marginal drop in performance (Figure 1). We also evaluate the proposed approach for video object segmentation and demonstrate its *generalization capability*.

2 Related work

Recent works on action detection in videos uses a CNN based approach [27, 28, 8, 9, 29] to perform spatio-temporal localization of actors in videos. A common and effective theme is the two-stage approach using object detection methods [30, 28, 31, 32, 33] to detect actors per frame based on action classification models [15, 34, 35, 36, 37, 38, 39] and combine them into tubes using temporal aggregation [10, 8, 27, 11, 7] for classification. While some works need a separate region proposal network to detect potential actors [8, 40], using a complicated two-stage process, other recent works have proposed simplified single-stage approach [9, 41]. As our work is centered around AL for selective annotation, we prefer a single-stage approach for an efficient solution.

Weak supervision: Large datasets for action detection require costly annotations, therefore innovative approaches have been proposed for this task with weak and semi-supervised methods. Some of these works have been able to reduce annotation cost significantly for action detection [20, 24, 25, 42] by using only the video-level annotation. Other methods have proposed the use of dense point-level pseudo-annotations [21] or only few bounding-box per instance [23] with the same objective. A common drawback of these methods is the inferior performance compared to fully supervised methods, which limits their practical utility.

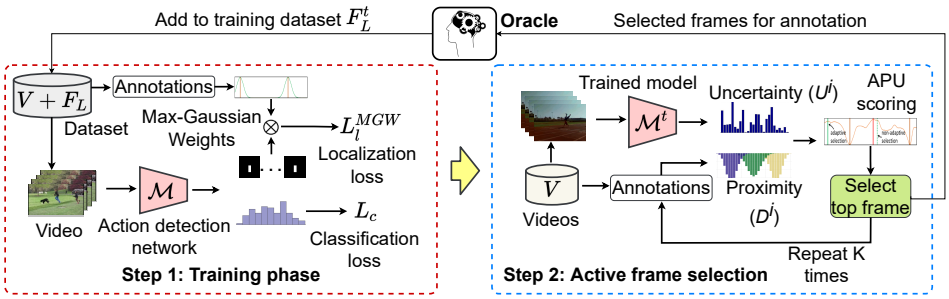

Figure 2: Overview of proposed approach. It consists of training and selection. During training the network is trained using existing annotations from the training set using *MGW-loss* to handle the sparse annotations. During iterative *APU* selection phase, the trained network is used to predict localizations on each frame of videos in the training set. Using these predictions, *APU* computes a score for each frame in a video to rank them and top *K* frames are sent to oracle for annotation.

Active learning: Active learning has been used to iteratively select unlabeled data for assigning labels based on certain utility factors [43, 44, 45, 46, 47]. Labeling a large set of data can often prove to be expensive and unnecessary, which is why AL can be vital in selecting related unlabeled data for further annotation in an iterative fashion. AL algorithms use uncertainty [46, 48, 49, 50, 51, 52], entropy [53, 54], heuristics and mutual information [45, 55, 56], core-set selection [57, 58] to select samples which are most likely to provide maximum utility to the learning algorithm. AL based classification algorithms are effective for different modalities such as images [45, 46, 44], videos [59, 60, 61], text [62, 63, 64] and speech [65]. Classification only needs class labels for an entire sample, making the scoring easier for the algorithm. However, extending that to a complex task such as object detection is challenging as it requires dense annotations in each sample [53, 66, 67, 68]. Extending that to videos adds extra level of complexities as it requires spatio-temporal annotations and selecting parts of video for extra annotation via AL algorithm is challenging. [69] performs frame selection using AL for object segmentation but does not leverage temporal aspect of video for avoiding sequential annotation, increasing overall annotation cost. There are *no existing methods* which focus on the problem of *active sparse labeling* in videos for *spatio-temporal detection task* and existing deep AL approaches are not applicable directly for this task.

3 Proposed method

We aim at reducing the annotation cost for labeling a set of videos $\mathcal{V} = \{V_1, ...V_N\}$ with N videos to learn an action detection model $\mathcal{M}$. We start with an initial set of sparse labels $\mathcal{S}_L^0 = \{V_{cls}, F_L^0\}$ that consists of annotated frames with class label V_{cls}, where only a small number of frames F_L^0 are annotated. This initial set of sparsely annotated videos is used to initialize an action detection model $\mathcal{M}^0$. This initialized model $\mathcal{M}^0$ is then used to estimate a utility score for all the unlabeled frames F_U^0 from the set of videos $\mathcal{V}$. The goal is to automatically select frames from unlabeled set to be manually labeled and obtain new set of sparse labels $\mathcal{S}_S^0$ which is merged with $\mathcal{S}_L^0$ for a new labeled set $\mathcal{S}_L^1$. The number of additional frames are selected based on a total budget B and they are annotated by an oracle (e.g. human annotator). The action detection model $\mathcal{M}$ is retrained using the new annotation set $\mathcal{S}_L^1$ and an updated model $\mathcal{M}^1$ is obtained. This process is repeated until we find a set $\mathcal{S}_L^F$ with several annotated frames in the videos $\mathcal{V}$ such that $\mathcal{M}^{\mathcal{F}}$ meets the target performance or the total budget B is exhausted. An overview of the proposed approach is shown in figure 2.

3.1 Active sparse labeling

Sparse labeling: We hypothesize that some frames will have more utility than others for learning action detection due to several factors, such as lack of motion, variation in action dynamics, redundancy in appearance or redundancy in action. In sparse labeling, we annotate only l frames $f_{v,l}$ in a video v instead of labelling all of them, leaving a set of u unannotated frames $f_{v,u}$. Therefore, it avoids annotation of frames with lower utility and helps in reducing the overall labeling cost. Each video v has a class label, denoted as v_{cls}, for the action category and a set of l annotated frames $f_{v,l}$ which indicates the localization of actions.

Uncertainty as frame utility: In each AL cycle, our goal is to select video frames for labeling which will have the highest utility for learning action detection. Uncertainty provides a measure to estimate model's confidence on its decision and has been used for selecting informative samples in existing works [70, 71, 72, 61]. These works are focused on classification and therefore the uncertainty is computed for the entire sample. Instead, we require informativeness of each frame in a video which is different from these works as it is computed for partial sample. The action detection model $\mathcal{M}$ provides spatio-temporal localization for the entire video and we propose to use the pixel-wise confidence score of localization on each frame to estimate frame-level uncertainty. We use MC-dropout [73] to estimate the model's uncertainty for each pixel in the video. MC-dropout is a more efficient form of uncertainty estimation compared to using a Bayesian neural network and is easier to implement [73, 74]. The uncertainty is estimated over T different trials and this score is averaged over all the pixels in a frame. For a given video v with I frames, the uncertainty U^i for the ith frame over T trials is computed as,

$$U^{i\in[1,I]} = \frac{1}{I^p}\sum_{h=1}^{I^p}\frac{1}{T}\sum_{j=1}^{T} -log(P(v_h^i, j)) \tag{1}$$

where I^p is the total number of pixels in a frame, and $P(v_h^i, j)$ represents the model prediction for h^{th} pixel in the ith frame of video v during the jth trial.

Adaptive proximity-aware uncertainty: Unlike images, the motion in videos has some continuity and it is highly likely that the frames close to each other will have similar uncertainty scores. Therefore selecting frames merely based on uncertainty will favor adjacent frames which may have similar utility for learning action detection. To overcome this issue, we propose a selection mechanism, termed as *Adaptive Proximity-aware Uncertainty (APU)*, which ensures that the selected frames have diversity in the temporal domain. APU scoring incorporates a distance measure into cost estimation and uses their *proximity* to the existing annotated frames. As we select more frames, this distance measure should *adapt* to the additional selected frames. We use a normal distribution $\mathcal{N}(\mu, \sigma^2)$ for distance measure D, where each annotated frame has its own distribution centered around its temporal location in the video. Given a video with K annotated frames, the distance measure D^i for the ith frame of the video is computed as,

$$D^i = 1 - \sum_{j=1}^{K} \varphi_i^j e^{-\frac{1}{2}(\frac{i-\mu_j}{\sigma})^2}. \tag{2}$$

where D^i is distance measure for unannotated frame i from annotated frame j, the distribution $\mathcal{N}$ for j^{th} annotated frame is centered at frame j with μ_j mean and σ variance, and $\varphi_i^j \in [0, 1]$ is the mask to select the closest distribution for i^{th} frame. The value of mask φ_i^j will be 1 for j^{th} distribution if it is closest to the ith frame, otherwise it will be 0. APU scoring uses both uncertainty and proximity and therefore prefers frames with high uncertainty and ensures temporal diversity. The overall APU score $\mathcal{U}_{APU}^i$ for a given frame is computed as,

$$\mathcal{U}_{APU}^i = \lambda U^i + (1-\lambda) D^i \tag{3}$$

where λ is used to control the contribution from uncertainty and temporal diversity. It is set to 0.5 for equal contribution in our formulation where U, D are both normalized in range (0,1).

Informative frame selection: Once we get $\mathcal{U}_{APU}$ score for all the frames in $\mathcal{V}$ videos, we select the frame with highest score globally and then score the remaining frames again with the adapted distance measure. The re-scoring is necessary to reduce probability of picking frames around same region, since a region doing poorly is likely to have more frames which scored higher in the selection process. We only need to recompute the distance measure, which is computationally inexpensive. The entire selection algorithm is provided Appendix. Once we have F_{annot} frames selected as per our budget, they are annotated by an oracle and the training set is updated with these new annotations. This completes one AL cycle and the model $\mathcal{M}$ is trained using the updated annotations.

Non-activity suppression: If all pixels in a frame are considered to compute its utility, non-activity regions may negatively influence the score as the model easily determines background pixels compared to the actual action region in a frame. A low uncertainty score from background pixels

will lower the overall frame uncertainty even if the activity region has high uncertainty, especially in videos with a relatively larger background area as compared to the actual action region. Therefore, we ignore pixels which are predicted as background (true negatives and false negatives) with high confidence (using a threshold τ) when computing the frame-level uncertainty. This might exclude some foreground pixels (false negatives) from the uncertainty estimation. However, these pixels will not be useful even if we use them as they are predicted as background due to low uncertainty.

3.2 Learning from sparse labels

Given a video clip $V = \{f_1, f_2, ...f_N\}$ with N frames where K frames are annotated such that $K < N$, we have to detect the action through the entire clip. A traditional action detection network is trained with the help of two different objectives, a classification loss L_c for action category and a localization loss L_l for spatio-temporal detection [8]. The classification loss L_c is computed for the entire video clip and the localization loss is computed for every frame in the video.

Sparse labeling will not allow us to compute the localization loss L_l on every frame due to missing annotations. The localization loss L_l with sparse labeling can be computed as, $L_l = \sum_{i=1}^{N} \beta^i L_l^i$. Here, L_l^i represents localization loss in the ith frame and $\beta^i \in [0, 1]$ indicates masking, which will be 1 for annotated frames and 0 otherwise. The masking strategy only uses the annotated frames for learning, therefore it is not quite effective. In a contrastive approach, we can use all the frames for learning by generating their *pseudo-labels* with the help of interpolation of annotations from neighboring frames. This will allow us to use all the frames but incurs noise from the pseudo-labels.

Max-gaussian weighted loss: We propose a simple loss formulation which benefits from both, masking and pseudo-labels. We hypothesize that the pseudo-labels close to ground-truth labels will be more reliable. Based on this, we propose *Max-Gaussian Weighted Loss (MGW-Loss)* which discounts the approximated pseudo-labels as they will not be as reliable as the actual ground-truth. We compute localization loss for each frame using both available and pseudo-labels, where the pseudo-labels have a varying weight in the overall loss component. The approximated annotations will not have a similar weight as their distance from the annotated frames will vary. We use a mixture of Gaussian distribution $w \in \{1..W\} \sim \mathcal{N}_w(\mu_{gt}, \sigma^2)$ to assign the weight to each frame, given $gt \in \{1..K\}$ actual ground-truth frame location as the mean of the distribution and σ is the variance of the distribution. We define the weighted localization loss L_l^{MGW} as,

$$L_l^{MGW} = \sum_{i=1}^{N} (\sum_{j=1}^{K} \phi_j^i e^{-\frac{1}{2}(\frac{i-\mu_j}{\sigma})^2}) L_l^i. \tag{4}$$

Here L_l^i is the localization loss of ith frame for any video, μ_j is the frame location for j^{th} annotated frame, and $\phi_j^i \in [0, 1]$ is the mask to select the max distribution for i^{th} frame. The value of mask ϕ_j^i will be 1 for j^{th} distribution if it has the maximum probability among all Gaussians at location of ith frame, otherwise it will be 0. The value of σ controls the weighting mechanism and it has two extremes. The high variance is equivalent to interpolation where all the frames will have equal weights and low variance is equivalent to masking where weights of pseudo-labels will be 0. Details on influence of σ provided in appendix C.1.

3.3 Action detection model

Video action detection is a challenging problem and the existing methods usually follow a complex pipeline [8, 10, 75]. Region proposal based approach has been found to be exceedingly effective [40], which has also been extended to tube proposals [8, 10]. However, training these two-step methods is not efficient, especially when we have to develop an iterative framework for AL. We follow a simpler approach where classification and detection can be done in an end-to-end training [9]. We simplified VideoCapsuleNet [9] further and replaced the 3D routing with 2D routing [76] which makes it more efficient in terms of memory and training speed. We then added dropout layers for uncertainty and used *MGW-Loss* from Eq. 4 to handle sparse labels. To handle sparse labels, we get the frame-wise weight from max-Gaussian weighted method and adjust the loss using this weight. Following [9], the network is trained using margin-loss for classification and binary-cross entropy loss for spatio-temporal localization.

Table 1: Comparison between different baseline methods in UCF-101 and J-HMDB dataset for different frame annotation percent. * is extended to video action detection using same backbone detector network as ours. [G: Gal et al.[73], A: Aghdam et al.[53]]

	UCF-101						J-HMDB					
	f-mAP@0.5			v-mAP@0.5			f-mAP@0.5			v-mAP@0.5		
Method	1%	5%	10%	1%	5%	10%	3%	6%	9%	9%	6%	9%
Random	60.7	66.5	69.3	59.2	66.4	69.9	58.3	69.3	71.6	57.4	64.6	70.4
Equidistant	61.8	66.2	68.4	61.7	67.2	69.0	57.4	67.5	71.4	56.9	64.9	66.8
G* [73]	60.9	66.7	68.9	59.4	66.8	69.1	58.2	66.7	67.5	57.4	66.8	67.4
A* [53]	61.4	67.9	69.8	60.1	67.9	70.0	58.8	71.2	71.1	57.7	66.7	71.2
Our	**64.7**	**70.9**	**71.7**	**63.9**	**71.8**	**73.2**	**68.8**	**74.1**	**74.5**	**65.6**	**70.8**	**74.0**

4 Experiments

Datasets and evaluation metrics: We evaluate our approach on three different datasets, **UCF-101** [13], **J-HMDB** [14] and **YouTube-VOS** [77]. UCF-101 has 3207 videos from 24 different classes with spatio-temporal bounding box annotations. J-HMDB dataset contains 928 videos from 21 classes with pixel-level spatio-temporal annotations. AVA [78] is a large-scale dataset with focus on action detection on single keyframe. This makes AVA not suitable for sparse frame selection as it does not provide spatio-temporal annotations. Similarly, MAMA [79] is a challenging dataset with low baseline detection scores (<1%), limiting sparse annotation study. We further evaluate our method on **YouTube-VOS** [77] for video object segmentation to demonstrate its generalization capability. YouTube-VOS consists of 3471 training videos (65 categories) with pixel-level annotation for multi-object segmentation. Following prior action detection works [80, 22] on UCF-101 and J-HMDB datasets, we compute the spatial IoU for each frame per class to get the frame average precision score and compute the spatio-temporal IoU per video per class to get the video average precision score score. This is then averaged to obtain the f-mAP and v-mAP scores over various thresholds. For video segmentation, we evaluate the avg. IoU ($\mathcal{J}score$) and the avg. boundary similarity ($\mathcal{F}score$) [77].

Implementation details: We implement our method in PyTorch [81]. In video action detection architecture, we use I3D encoder head [15] with pre-trained weights from the Charades dataset [82]. We use Adam optimizer [83] with a batch size of 8 and train for 22K iterations in each active learning cycle (details in appendix G.3). We use dropout for generating uncertainty similar to [73] by enabling it during inference. For YouTube-VOS task, we use two existing methods [77, 84]. We use $\tau = 0.9$ for non-active suppression and $\sigma = 1.3$ for Eq. 2 and Eq. 4, which were empirically determined (details in appendix C).

Sparse learning settings: In the initialization stage, we assume the availability of annotations for $I\%$ of frames in each video in $\mathcal{V}$ to make sparse annotation set $\mathcal{S}_L^0$. These frames are randomly selected for the first stage. We use 1%, 3%, and 5% initial frames for UCF-101, J-HMDB, and Youtube-VOS respectively, determined empirically based on each dataset size. We assign annotation cost for each frame as $C_{frame} = Actor \times Clicks$ based on clicks per actor (bounding box/pixels).

4.1 Baseline methods

We explore several baselines to understand their limitations on video action detection. First, we use random and equidistant frame selection where random selection select the frames at random in each stage, equidistant uses equal distance between the frames during selection. Next, we extend existing AL methods used in image-based object detection [53, 73] to video action detection, where we score each frame using their algorithm for frame selection. We improve upon the uncertainty sampling for video level selection from [61] and compute uncertainty at pixel-level in all our baselines. We train all baselines using same action detection backbone for a fair comparison. We have random, equidistant, uncertainty-based [73] and entropy-based [53] approaches as baseline methods to compare against.

4.2 Results

Analysis of baseline methods: We evaluate random, equidistant, entropy-based [53] and uncertainty-based [73] selection methods as baselines and compare with our approach in Table 1. While all baselines are effective for AL in image-based detection/classification tasks, we demonstrate that for video action detection prior methods [53, 73] perform similar or worse than random

Table 2: Evaluation of the proposed method on **UCF-101** and **J-HMDB**.

UCF-101					**J-HMDB**				
Annot	v-mAP@		f-mAP@		Annot	v-mAP@		f-mAP@	
Percent	0.3	0.5	0.3	0.5	Percent	0.3	0.5	0.3	0.5
1%	89.01	63.94	83.85	64.69	3%	95.15	65.56	89.94	68.78
5%	90.95	71.89	88.71	70.91	6%	95.20	70.75	93.09	74.09
10%	91.12	73.20	88.72	71.75	9%	95.58	74.01	92.67	74.50
100%	91.49	75.15	89.08	74.02	100%	96.39	75.75	93.74	74.91

Table 3: Comparison with state-of-the-art methods. We evaluate our approach using v-mAP and f-mAP scores using only 10% annotations. 'Video' uses video-level class annotations and 'Partial' uses sparse temporal and spatial annotations. V: video labels, P: points, B: bounding box, O: off-the-shelf detector. **f@** denotes **f-mAP@**

Method	Annot					**UCF-101**					**J-HMDB**				
						f@	v-mAP@				f@	v-mAP@			
	Percent	V	P	B	O	0.5	0.1	0.2	0.3	0.5	0.5	0.1	0.2	0.3	0.5
Fully supervised															
Peng et al. [7]	100%					65.7	77.3	72.9	65.7	35.9	58.5	-	74.3	-	73.1
TCNN [8]	100%					67.3	77.9	73.1	69.4	-	61.3	-	78.4	-	-
Gu et al. [78]	100%					76.3	-	-	-	59.9	73.3	-	-	-	-
ACT [85]	100%					69.5	-	76.5	-	-	-	-	74.2	-	73.7
STEP [10]	100%					75.0	83.1	76.6	-	-	-	-	-	-	-
VidsCapsNet [9]	100%					78.6	98.6	97.1	93.7	80.3	64.6	98.4	95.1	89.1	61.9
Weakly/Semi-supervised															
Mettes et al. [20]	Video	✓			✓	-	-	37.4	-	-	-	-	-	-	-
Escorcia et al. [24]	Video	✓				-	-	45.5	-	-	-	-	-	-	-
Zhang et al. [25]	Video	✓			✓	30.4	62.1	45.5	-	17.3	65.9	81.5	77.3	-	50.8
Arnab et al. [42]	Video	✓			✓	-	-	61.7	-	35.0	-	-	-	-	-
Weinz. et al. [26]	Partial	✓		✓	✓	63.8	-	57.3	-	46.9	56.5	-	-	-	64.0
Mettes et al. [21]	Partial	✓	✓			-	-	41.8	-	-	-	-	-	-	-
Cheron et al. [23]	Partial	✓			✓	-	-	70.6	-	38.6	-	-	-	-	-
Kumar et al. [86]	20%	✓		✓		69.9	-	95.7	-	72.1	64.4	-	95.4	-	63.5
Ours	10%	✓		✓		71.7	98.1	96.5	91.1	73.2	74.5	99.2	98.4	95.6	74.0
Ours	100%					74.0	98.3	96.9	91.5	75.2	74.9	99.2	99.2	96.4	75.8

or equidistant methods. The lack of temporal information prohibits prior methods to select frames effectively as videos have sequential frames in same region with high uncertainty. Our approach accounts for the temporal continuity and outperforms all baselines including prior AL based methods [73, 53] consistently on both dataset for all annotation percent. This demonstrates that extending image-based methods are not well suited for video action detection task as shown in Figure 3.

Evaluation of proposed method: We evaluate our approach on UCF-101 and J-HMDB for action detection and compare with fully-supervised training in Table 2. For **UCF-101** we initialize with 1% of labelled frames and train the action detection model with a step size of 5% in each cycle. We achieve results very close to full annotations (v-mAP@0.5, 73.20 vs 75.12) using only 10% of annotated frames, which is a huge reduction (90%) in the annotation cost. For **J-HMDB**, we initialize with 3% labels as it is a relatively smaller dataset and it is challenging to train an initial model with just 1% labels. Here, we obtain results comparable with 100% annotations with only 9% of labels.

Comparison to prior weakly/semi-supervised approach: We compare to prior weakly/semi-supervised action detection approach [23, 24, 21, 20, 26, 86] in Table 3 and explain their limitations. [26] uses external human and instance detectors to build tubes aligned with 1-5 random spatially annotated GT frames per tube. This incurs larger annotation cost without any frame selection metric while having low performance. [20, 21, 42] follow Multi Instance Learning (MIL) approach, where [20] uses off-the-shelf actor detectors to generate pseudo-annotations and [21] relies on user input for point annotation *for every frame*, requiring large annotation cost. [42] expands on MIL approach combined with tubelets generated by an off-the-shelf human detector. While MIL based approach requires less oversight, it also suffers from reduced performance, even with state-of-the-art detectors.

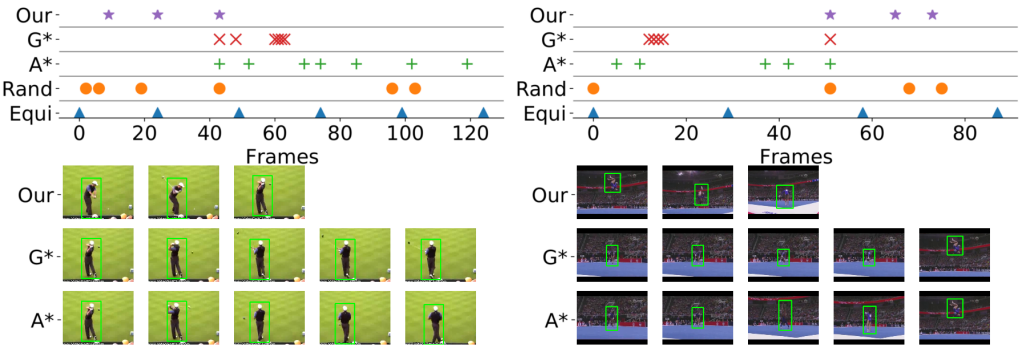

Figure 3: Analysis of frame selection using different methods. The x-axis represents all frames of the video, with each row representing a baseline method. The markers for each method mark the frames selected using that method. For both samples, our method selects distributed frames centered around action region, Gal et al [73] **[G*]** selects frame around same region since there is no distance measure and Aghdam et al. [53] **[A*]** selects slightly more distributed frames but those are not from crucial action region. [G*:Gal et al[73], A*:Aghdam et al[53], Rand: Random, Equi: Equidistant]

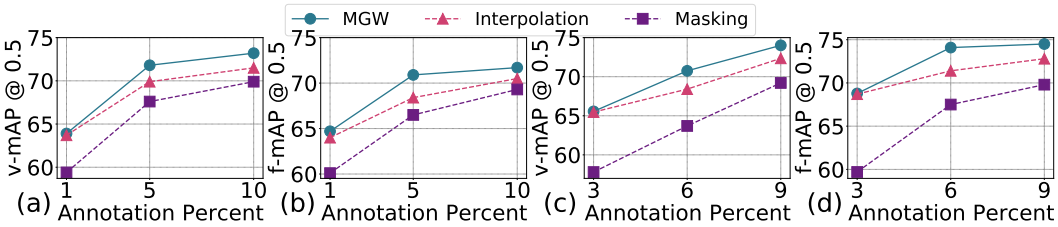

Figure 4: Comparison of different loss functions for UCF-101 (a-b) and J-HMDB (c-d).

[24] uses actor detector with video-level label to perform action detection, using a less involved approach as [42], but both have high label noise and low performance. [86] uses consistency regularization to train with unlabeled data in semi-supervised fashion. [23] uses discriminative clustering instead of MIL to assign tubelets to action label with various level of supervision, [25] uses combination of different actor detectors to build tube to train with video labels. They rely on multiple off-the-shelf components to generate the tubelets and suffer from low performance. [25] and [26] report their J-HMDB results using bounding-box annotation instead of the fine-grained pixel-wise annotation due to their design limitation to use external bounding-box detector for tube generation. Our approach does not rely on such detectors and can work with both bounding-box (UCF-101) and pixel-wise (J-HMDB) annotation and is comparable to the supervised performance.

4.3 Ablations

Effect of loss function: We evaluate the effectiveness of *MGW-Loss* for video action detection with sparse labels and compare it with baseline masking and interpolation based loss in figure 4. The proposed *MGW-Loss* learns better in sparse label conditions due to the approximated ground truth frames from interpolation. Without the approximated frames, the formulation in Eq. 4 will reduce to masking loss as $\sigma \rightarrow 0$. Masking computes loss only on the sparse ground truth and does not perform as well as the *MGW-loss* with interpolated ground truth as seen in figure 4. Our Gaussian based interpolation adapts better for approximated labels compared with simple interpolation due to having different weight for each frame based on their distance from real ground truth annotation.

Effect of selection criteria: We compare how commonly used entropy and uncertainty-based selection methods perform against proposed *APU* algorithm when using the same loss formulation from Eq. 4. Figure 5 shows that *APU* has optimum frame selection as it encourages diverse selection by using adaptive distance to existing frames for the scoring process. Following [53], entropy based selection has a less effective fixed distance filter to avoid nearby frames. The uncertainty method

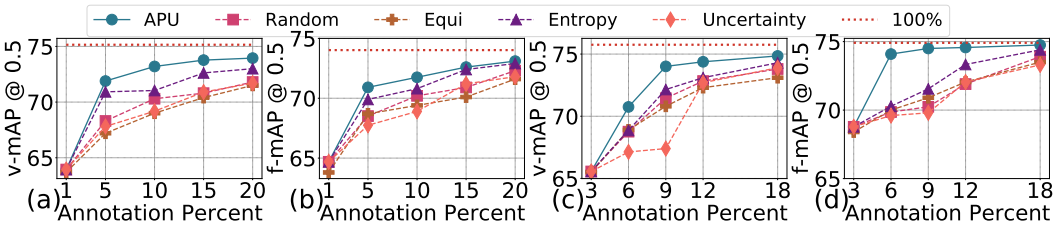

Figure 5: Comparison of different frame selection methods combined with MGW-Loss showing v-mAP and f-mAP scores for IoU @ 0.5 for (a-b) UCF-101 evaluation up to 20% (∼40k frames) data annotation. (c-d) J-HMDB evaluation up to 18% (∼3800 frames). Our *APU* approach gets better performance at a lower annotation percentage (lower annotation cost).

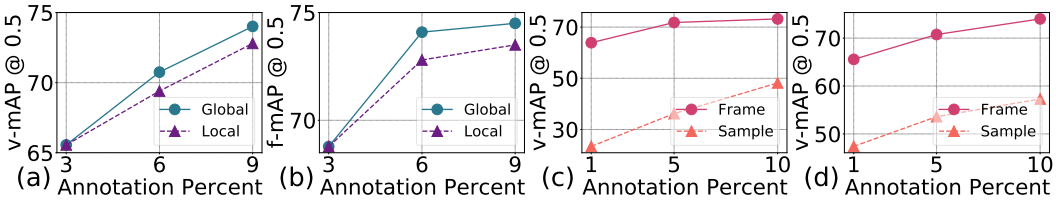

Figure 6: Analysis on sample selection strategy. (a-b) Global vs local frame selection strategy using *APU* on J-HMDB. (c-d) Frame vs sample selection for UCF-101 (c) and J-HMDB(d).

lacks any distance component and performs worse than random or equidistant, selecting frames from nearby regions as seen in figure 3.

Annotating more frames We also evaluate adding additional frames until the scores start to saturate, shown in figure 5. We see that for UCF-101 at 20% annotation (∼40k frames) all methods score close to each other. Similarly, J-HMDB dataset has similar convergence pattern at 18% annotation (∼3800 frames). This demonstrates that while the frame selection eventually converges with more data, our approach gets better score at an earlier stage, saving overall annotation cost.

4.4 Discussions

Variation in budget steps: Lower budget steps enables selection of fewer frames with high utility in each step instead of selecting more frames with low utility in higher budget steps. As the annotation set is more curated in each step in lower steps, we end up with better frames for the same annotation budget as higher steps. We evaluate the effect of using step size of 1% and 5% in figure 1 for UCF-101 dataset, starting from 1% till 10%. Step size of 1% has constantly better v-mAP and f-mAP score throughout, showing that smaller steps give greater performance. However, smaller step size needs more iterations, taking more time as a trade-off for better performance.

Local vs. global selection: The proposed approach is focused on sparse labeling where frames with high utility within a video are selected for annotations. However, it is important to note that videos as a whole have varying utility. To exploit this aspect, we explore two different frame selection strategies, local selection and global selection. In local selection, each video has a fixed budget b/N^v, where b is budget per cycle and N^v is the total number of videos in our training set. However, frames in global selection are taken from a global pool which includes frames from all videos, ranking based on overall dataset utility. Figure 6 (a-b) shows that global selection outperforms local selection strategy, emphasizing that some videos can be more informative than others as confirmed in figure 7.

Sample vs. frame selection: We follow [21] and annotate the entire sample (video) instead of finding the most useful frames within each sample. We compute pixel level uncertainty which is averaged over all the pixels in a frame using Eq. 1 and then averaged over all frames in a video to get the video level score. While this approach is simpler, it has higher cost during annotation with lower data variation. Let us assume a fixed cost of c per frame with f frames to annotate, we can assume a budget of $B = c \times f$. We could distribute the frames across the set by picking only few

Figure 7: Sparse selection analysis. (a) Histogram showing number of frames selected per video using our method on UCF-101. Videos on the right show two samples from extreme ends of this histogram as marked in the plot. (b) Samples for cricket bowling class with APU selected frames on red marker (APU selects only two frames for 1 action instance). (c) Samples for salsa spin class (APU selects multiple frames (red) as each spin instance is visually diverse).

Table 4: Comparison of the proposed method on YouTube-VOS dataset with baseline AL methods using STCN [84]. A = Aghdam et al. [53], G = Gal et al. [73]. * is extended to video object segmentation using same network as ours.

	Overall			$\mathcal{J}_S$			$\mathcal{J}_U$			$\mathcal{F}_S$			$\mathcal{F}_U$		
Method	10%	20%	30%	10%	20%	30%	10%	20%	30%	10%	20%	30%	10%	20%	30%
Random	28.4	42.3	42.5	29.1	42.9	43.8	25.8	38.5	38.6	30.2	44.3	45.0	28.4	43.5	42.7
A * [53]	30.1	45.6	47.2	31.5	45.4	47.6	26.7	43.4	47.9	22.8	46.7	48.8	17.6	46.8	44.6
G * [73]	27.9	45.1	48.8	28.5	50.8	48.5	24.8	42.0	46.6	29.7	42.1	49.8	28.7	45.5	50.4
Our	**31.7**	**58.6**	**66.7**	**33.6**	**58.2**	**66.7**	**27.8**	**54.3**	**61.5**	**35.2**	**60.6**	**69.1**	**30.1**	**60.9**	**69.7**

important frames from each video, which would increase variation in the training set. However, if we annotate entire sample, there will be many redundant annotations with little gain, which is why frame selection performs better for action detection task as observed in figure 6 (c-d).

4.5 Generalization beyond action detection

We test generalization of proposed cost and loss function for video object segmentation task on the YouTube-VOS 2019. Table 4 shows that our proposed selection approach gets better $\mathcal{J}$ and $\mathcal{F}$ scores for video segmentation task compared to baseline AL methods and random frame selection method. We provide further details in appendix F and G.2.

4.6 Limitations

As most AL methods, this approach reduces annotation cost with multiple selection iterations, being more time consuming compared to weakly-supervised approaches. As we only measure frames within same video, future work can focus on evaluating each video's utility as well for the task.

5 Conclusion

In this work we present active sparse labeling (ASL), a novel approach for label-efficient video action detection. The proposed approach uses an uncertainty-based scoring mechanism for selecting informative and diverse set of frames for action detection. In addition, we also propose a simple yet effective loss formulation which can be used to train a model with sparse labels. The proposed approach is promising in saving annotation costs and we show that merely 10% of labels can achieve performance comparable to fully supervised methods. We further demonstrate the generalization capability of the proposed approach for video object segmentation.

6 Acknowledgements

This research is based upon work supported in part by the Office of the Director of National Intelligence (Intelligence Advanced Research Projects Activity) via 2022-21102100001 and in part by University of Central Florida seed funding. The views and conclusions contained herein are those of the authors and should not be interpreted as necessarily representing the official policies, either expressed or implied, of ODNI, IARPA, or the US Government. The US Government is authorized to reproduce and distribute reprints for governmental purposes notwithstanding any copyright annotation therein.

References

[1] Joshua Gleason, Carlos D Castillo, and Rama Chellappa. Real-time detection of activities in untrimmed videos. In *Proceedings of the IEEE/CVF Winter Conference on Applications of Computer Vision Workshops*, pages 117–125, 2020.

[2] Mamshad Nayeem Rizve, Ugur Demir, Praveen Tirupattur, Aayush Jung Rana, Kevin Duarte, Ishan R Dave, Yogesh S Rawat, and Mubarak Shah. Gabriella: An online system for real-time activity detection in untrimmed security videos. In *2020 25th International Conference on Pattern Recognition (ICPR)*, pages 4237–4244. IEEE, 2021.

[3] Markus Schön, Michael Buchholz, and Klaus Dietmayer. Mgnet: Monocular geometric scene understanding for autonomous driving. In *Proceedings of the IEEE/CVF International Conference on Computer Vision*, pages 15804–15815, 2021.

[4] Di Feng, Christian Haase-Schütz, Lars Rosenbaum, Heinz Hertlein, Claudius Glaeser, Fabian Timm, Werner Wiesbeck, and Klaus Dietmayer. Deep multi-modal object detection and semantic segmentation for autonomous driving: Datasets, methods, and challenges. *IEEE Transactions on Intelligent Transportation Systems*, 22(3):1341–1360, 2020.

[5] Alex X Lee, Richard Zhang, Frederik Ebert, Pieter Abbeel, Chelsea Finn, and Sergey Levine. Stochastic adversarial video prediction. *arXiv preprint arXiv:1804.01523*, 2018.

[6] Chelsea Finn, Ian Goodfellow, and Sergey Levine. Unsupervised learning for physical interaction through video prediction. *arXiv preprint arXiv:1605.07157*, 2016.

[7] Xiaojiang Peng and Cordelia Schmid. Multi-region two-stream r-cnn for action detection. In *European conference on computer vision*, pages 744–759. Springer, 2016.

[8] Rui Hou, Chen Chen, and Mubarak Shah. Tube convolutional neural network (t-cnn) for action detection in videos. In *IEEE International Conference on Computer Vision*, 2017.

[9] Kevin Duarte, Yogesh Rawat, and Mubarak Shah. Videocapsulenet: A simplified network for action detection. In *Advances in Neural Information Processing Systems*, pages 7610–7619, 2018.

[10] Xitong Yang, Xiaodong Yang, Ming-Yu Liu, Fanyi Xiao, Larry S Davis, and Jan Kautz. Step: Spatio-temporal progressive learning for video action detection. In *Proceedings of the IEEE Conference on Computer Vision and Pattern Recognition*, pages 264–272, 2019.

[11] Dong Li, Zhaofan Qiu, Qi Dai, Ting Yao, and Tao Mei. Recurrent tubelet proposal and recognition networks for action detection. In *Proceedings of the European conference on computer vision (ECCV)*, pages 303–318, 2018.

[12] Kirill Gavrilyuk, Amir Ghodrati, Zhenyang Li, and Cees GM Snoek. Actor and action video segmentation from a sentence. In *Proceedings of the IEEE Conference on Computer Vision and Pattern Recognition*, pages 5958–5966, 2018.

[13] Khurram Soomro, Amir Roshan Zamir, and Mubarak Shah. Ucf101: A dataset of 101 human actions classes from videos in the wild. *arXiv preprint arXiv:1212.0402*, 2012.

[14] Hueihan Jhuang, Juergen Gall, Silvia Zuffi, Cordelia Schmid, and Michael J Black. Towards understanding action recognition. In *Proceedings of the IEEE international conference on computer vision*, pages 3192–3199, 2013.

[15] Joao Carreira and Andrew Zisserman. Quo vadis, action recognition? a new model and the kinetics dataset. In *proceedings of the IEEE Conference on Computer Vision and Pattern Recognition*, pages 6299–6308, 2017.

[16] Andrej Karpathy, George Toderici, Sanketh Shetty, Thomas Leung, Rahul Sukthankar, and Li Fei-Fei. Large-scale video classification with convolutional neural networks. In *CVPR*, 2014.

[17] Sami Abu-El-Haija, Nisarg Kothari, Joonseok Lee, Paul Natsev, George Toderici, Balakrishnan Varadarajan, and Sudheendra Vijayanarasimhan. Youtube-8m: A large-scale video classification benchmark. *arXiv preprint arXiv:1609.08675*, 2016.

[18] Ali Diba, Mohsen Fayyaz, Vivek Sharma, Manohar Paluri, Jürgen Gall, Rainer Stiefelhagen, and Luc Van Gool. Large scale holistic video understanding. In *European Conference on Computer Vision*, pages 593–610. Springer, 2020.

[19] Mathew Monfort, Alex Andonian, Bolei Zhou, Kandan Ramakrishnan, Sarah Adel Bargal, Tom Yan, Lisa Brown, Quanfu Fan, Dan Gutfruend, Carl Vondrick, et al. Moments in time dataset: one million videos for event understanding. *IEEE Transactions on Pattern Analysis and Machine Intelligence*, pages 1–8, 2019.

[20] Pascal Mettes, Cees GM Snoek, and Shih-Fu Chang. Localizing actions from video labels and pseudo-annotations. *arXiv preprint arXiv:1707.09143*, 2017.

[21] Pascal Mettes and Cees GM Snoek. Pointly-supervised action localization. *International Journal of Computer Vision*, 127(3):263–281, 2019.

[22] Philippe Weinzaepfel, Zaid Harchaoui, and Cordelia Schmid. Learning to track for spatio-temporal action localization. In *Proceedings of the IEEE international conference on computer vision*, pages 3164–3172, 2015.

[23] Guilhem Chéron, Jean-Baptiste Alayrac, Ivan Laptev, and Cordelia Schmid. A flexible model for training action localization with varying levels of supervision. In *Proceedings of the 32nd International Conference on Neural Information Processing Systems*, pages 950–961, 2018.

[24] Victor Escorcia, Cuong D Dao, Mihir Jain, Bernard Ghanem, and Cees Snoek. Guess where? actor-supervision for spatiotemporal action localization. *Computer Vision and Image Understanding*, 192:102886, 2020.

[25] Shiwei Zhang, Lin Song, Changxin Gao, and Nong Sang. Glnet: Global local network for weakly supervised action localization. *IEEE Transactions on Multimedia*, 22(10):2610–2622, 2019.

[26] Philippe Weinzaepfel, Xavier Martin, and Cordelia Schmid. Human action localization with sparse spatial supervision. *arXiv preprint arXiv:1605.05197*, 2016.

[27] Zhenheng Yang, Jiyang Gao, and Ram Nevatia. Spatio-temporal action detection with cascade proposal and location anticipation. In *Proceedings of the British Machine Vision Conference (BMVC)*, 2017.

[28] Georgia Gkioxari, Ross Girshick, Piotr Dollár, and Kaiming He. Detecting and recognizing human-object interactions. In *Proceedings of the IEEE Conference on Computer Vision and Pattern Recognition*, pages 8359–8367, 2018.

[29] Aayush J. Rana and Yogesh S. Rawat. We don't need thousand proposals: Single shot actor-action detection in videos. In *Proceedings of the IEEE/CVF Winter Conference on Applications of Computer Vision (WACV)*, pages 2960–2969, January 2021.

[30] Shaoqing Ren, Kaiming He, Ross Girshick, and Jian Sun. Faster r-cnn: Towards real-time object detection with region proposal networks. In *Advances in neural information processing systems*, pages 91–99, 2015.

[31] Joseph Redmon, Santosh Divvala, Ross Girshick, and Ali Farhadi. You only look once: Unified, real-time object detection. In *Proceedings of the IEEE conference on computer vision and pattern recognition*, pages 779–788, 2016.

[32] Joseph Redmon and Ali Farhadi. Yolo9000: better, faster, stronger. *arXiv preprint*, 1612, 2016.

[33] Wei Liu, Dragomir Anguelov, Dumitru Erhan, Christian Szegedy, Scott Reed, Cheng-Yang Fu, and Alexander C Berg. Ssd: Single shot multibox detector. In *European conference on computer vision*, pages 21–37. Springer, 2016.

[34] Kensho Hara, Hirokatsu Kataoka, and Yutaka Satoh. Can spatiotemporal 3d cnns retrace the history of 2d cnns and imagenet? In *Proceedings of the IEEE conference on Computer Vision and Pattern Recognition*, pages 6546–6555, 2018.

[35] Zhaofan Qiu, Ting Yao, and Tao Mei. Learning spatio-temporal representation with pseudo-3d residual networks. In *proceedings of the IEEE International Conference on Computer Vision*, pages 5533–5541, 2017.

[36] Saining Xie, Chen Sun, Jonathan Huang, Zhuowen Tu, and Kevin Murphy. Rethinking spatiotemporal feature learning: Speed-accuracy trade-offs in video classification. In *Proceedings of the European Conference on Computer Vision (ECCV)*, pages 305–321, 2018.

[37] Du Tran, Lubomir Bourdev, Rob Fergus, Lorenzo Torresani, and Manohar Paluri. Learning spatiotemporal features with 3d convolutional networks. In *Computer Vision (ICCV), 2015 IEEE International Conference on*, pages 4489–4497. IEEE, 2015.

[38] Karen Simonyan and Andrew Zisserman. Two-stream convolutional networks for action recognition in videos. In *Advances in neural information processing systems*, pages 568–576, 2014.

[39] Shruti Vyas, Yogesh S Rawat, and Mubarak Shah. Multi-view action recognition using cross-view video prediction. In *Proceedings of the European Conference on Computer Vision*, 2020.

[40] Rohit Girdhar, Joao Carreira, Carl Doersch, and Andrew Zisserman. Video action transformer network. In *Proceedings of the IEEE Conference on Computer Vision and Pattern Recognition*, pages 244–253, 2019.

[41] Jiaojiao Zhao, Xinyu Li, Chunhui Liu, Shuai Bing, Hao Chen, Cees GM Snoek, and Joseph Tighe. Tuber: Tube-transformer for action detection. *arXiv preprint arXiv:2104.00969*, 2021.

[42] Anurag Arnab, Chen Sun, Arsha Nagrani, and Cordelia Schmid. Uncertainty-aware weakly supervised action detection from untrimmed videos. In *European Conference on Computer Vision*, pages 751–768. Springer, 2020.

[43] Burr Settles. Active learning literature survey. 2009.

[44] Xin Li and Yuhong Guo. Adaptive active learning for image classification. In *Proceedings of the IEEE Conference on Computer Vision and Pattern Recognition*, pages 859–866, 2013.

[45] Keze Wang, Dongyu Zhang, Ya Li, Ruimao Zhang, and Liang Lin. Cost-effective active learning for deep image classification. *IEEE Transactions on Circuits and Systems for Video Technology*, 27(12):2591–2600, 2016.

[46] Ajay J Joshi, Fatih Porikli, and Nikolaos Papanikolopoulos. Multi-class active learning for image classification. In *2009 IEEE Conference on Computer Vision and Pattern Recognition*, pages 2372–2379. IEEE, 2009.

[47] Pengzhen Ren, Yun Xiao, Xiaojun Chang, Po-Yao Huang, Zhihui Li, Brij B Gupta, Xiaojiang Chen, and Xin Wang. A survey of deep active learning. *ACM Computing Surveys (CSUR)*, 54(9):1–40, 2021.

[48] Guang Zhao, Edward Dougherty, Byung-Jun Yoon, Francis Alexander, and Xiaoning Qian. Uncertainty-aware active learning for optimal bayesian classifier. In *International Conference on Learning Representations (ICLR 2021)*, 2021.

[49] Yarin Gal, Riashat Islam, and Zoubin Ghahramani. Deep bayesian active learning with image data. In *International Conference on Machine Learning*, pages 1183–1192. PMLR, 2017.

[50] William H Beluch, Tim Genewein, Andreas Nürnberger, and Jan M Köhler. The power of ensembles for active learning in image classification. In *Proceedings of the IEEE conference on computer vision and pattern recognition*, pages 9368–9377, 2018.

[51] Ashish Kapoor, Kristen Grauman, Raquel Urtasun, and Trevor Darrell. Active learning with gaussian processes for object categorization. In *2007 IEEE 11th international conference on computer vision*, pages 1–8. IEEE, 2007.

[52] Zimo Liu, Jingya Wang, Shaogang Gong, Huchuan Lu, and Dacheng Tao. Deep reinforcement active learning for human-in-the-loop person re-identification. In *Proceedings of the IEEE/CVF International Conference on Computer Vision*, pages 6122–6131, 2019.

[53] Hamed H Aghdam, Abel Gonzalez-Garcia, Joost van de Weijer, and Antonio M López. Active learning for deep detection neural networks. In *Proceedings of the IEEE/CVF International Conference on Computer Vision*, pages 3672–3680, 2019.

[54] Alex Holub, Pietro Perona, and Michael C Burl. Entropy-based active learning for object recognition. In *2008 IEEE Computer Society Conference on Computer Vision and Pattern Recognition Workshops*, pages 1–8. IEEE, 2008.

[55] Andreas Kirsch, Joost Van Amersfoort, and Yarin Gal. Batchbald: Efficient and diverse batch acquisition for deep bayesian active learning. *Advances in neural information processing systems*, 32, 2019.

[56] Neil Houlsby, Ferenc Huszár, Zoubin Ghahramani, and Máté Lengyel. Bayesian active learning for classification and preference learning. *arXiv preprint arXiv:1112.5745*, 2011.

[57] Ozan Sener and Silvio Savarese. Active learning for convolutional neural networks: A core-set approach. *arXiv preprint arXiv:1708.00489*, 2017.

[58] Robert Pinsler, Jonathan Gordon, Eric Nalisnick, and José Miguel Hernández-Lobato. Bayesian batch active learning as sparse subset approximation. *Advances in Neural Information Processing Systems*, 32, 2019.

[59] Carl Vondrick and Deva Ramanan. Video annotation and tracking with active learning. *Advances in Neural Information Processing Systems*, 24:28–36, 2011.

[60] Javad Zolfaghari Bengar, Abel Gonzalez-Garcia, Gabriel Villalonga, Bogdan Raducanu, Hamed Habibi Aghdam, Mikhail Mozerov, Antonio M López, and Joost van de Weijer. Temporal coherence for active learning in videos. In *Proceedings of the IEEE/CVF International Conference on Computer Vision Workshops*, pages 0–0, 2019.

[61] Fabian Caba Heilbron, Joon-Young Lee, Hailin Jin, and Bernard Ghanem. What do i annotate next? an empirical study of active learning for action localization. In *Proceedings of the European Conference on Computer Vision (ECCV)*, pages 199–216, 2018.

[62] Bishan Yang, Jian-Tao Sun, Tengjiao Wang, and Zheng Chen. Effective multi-label active learning for text classification. In *Proceedings of the 15th ACM SIGKDD international conference on Knowledge discovery and data mining*, pages 917–926, 2009.

[63] Ye Zhang, Matthew Lease, and Byron Wallace. Active discriminative text representation learning. In *Proceedings of the AAAI Conference on Artificial Intelligence*, volume 31, 2017.

[64] Ameya Prabhu, Charles Dognin, and Maneesh Singh. Sampling bias in deep active classification: An empirical study. *arXiv preprint arXiv:1909.09389*, 2019.

[65] Dilek Hakkani-Tür, Giuseppe Riccardi, and Allen Gorin. Active learning for automatic speech recognition. In *2002 IEEE international conference on acoustics, speech, and signal processing*, volume 4, pages IV–3904. IEEE, 2002.

[66] Soumya Roy, Asim Unmesh, and Vinay P Namboodiri. Deep active learning for object detection. In *BMVC*, page 91, 2018.

[67] Jiwoong Choi, Ismail Elezi, Hyuk-Jae Lee, Clement Farabet, and Jose M Alvarez. Active learning for deep object detection via probabilistic modeling. In *Proceedings of the IEEE/CVF International Conference on Computer Vision*, pages 10264–10273, 2021.

[68] Tianning Yuan, Fang Wan, Mengying Fu, Jianzhuang Liu, Songcen Xu, Xiangyang Ji, and Qixiang Ye. Multiple instance active learning for object detection. In *Proceedings of the IEEE/CVF Conference on Computer Vision and Pattern Recognition*, pages 5330–5339, 2021.

[69] Alireza Fathi, Maria Florina Balcan, Xiaofeng Ren, and James M Rehg. Combining self training and active learning for video segmentation. In *Proceedings of the British Machine Vision Conference (BMVC)*, 2011.

[70] Prateek Jain and Ashish Kapoor. Active learning for large multi-class problems. In *2009 IEEE Conference on Computer Vision and Pattern Recognition*, pages 762–769. IEEE, 2009.

[71] Xin Li and Yuhong Guo. Adaptive active learning for image classification. In *Proceedings of the IEEE Conference on Computer Vision and Pattern Recognition*, pages 859–866, 2013.

[72] Yi Yang, Zhigang Ma, Feiping Nie, Xiaojun Chang, and Alexander G Hauptmann. Multi-class active learning by uncertainty sampling with diversity maximization. *International Journal of Computer Vision*, 113(2):113–127, 2015.

[73] Yarin Gal and Zoubin Ghahramani. Dropout as a bayesian approximation: Representing model uncertainty in deep learning. In *International Conference on Machine Learning*, pages 1050–1059. PMLR, 2016.

[74] Mamshad Nayeem Rizve, Kevin Duarte, Yogesh S Rawat, and Mubarak Shah. In defense of pseudo-labeling: An uncertainty-aware pseudo-label selection framework for semi-supervised learning. In *International Conference on Learning Representations*, 2021.

[75] Rui Hou, Chen Chen, and Mubarak Shah. An end-to-end 3d convolutional neural network for action detection and segmentation in videos. *arXiv preprint arXiv:1712.01111*, 2017.

[76] Geoffrey E Hinton, Sara Sabour, and Nicholas Frosst. Matrix capsules with em routing. In *International conference on learning representations*, 2018.

[77] Ning Xu, Linjie Yang, Yuchen Fan, Jianchao Yang, Dingcheng Yue, Yuchen Liang, Brian Price, Scott Cohen, and Thomas Huang. Youtube-vos: Sequence-to-sequence video object segmentation. In *Proceedings of the European Conference on Computer Vision (ECCV)*, pages 585–601, 2018.

[78] Chunhui Gu, Chen Sun, David A Ross, Carl Vondrick, Caroline Pantofaru, Yeqing Li, Sudheendra Vijayanarasimhan, George Toderici, Susanna Ricco, Rahul Sukthankar, et al. Ava: A video dataset of spatio-temporally localized atomic visual actions. In *Proceedings of the IEEE Conference on Computer Vision and Pattern Recognition*, pages 6047–6056, 2018.

[79] Rajat Modi, Aayush Jung Rana, Akash Kumar, Praveen Tirupattur, Shruti Vyas, Yogesh Rawat, and Mubarak Shah. Video action detection: Analysing limitations and challenges. In *Proceedings of the IEEE/CVF Conference on Computer Vision and Pattern Recognition*, pages 4911–4920, 2022.

[80] Georgia Gkioxari and Jitendra Malik. Finding action tubes. In *Proceedings of the IEEE conference on computer vision and pattern recognition*, pages 759–768, 2015.

[81] Adam Paszke, Sam Gross, Francisco Massa, Adam Lerer, James Bradbury, Gregory Chanan, Trevor Killeen, Zeming Lin, Natalia Gimelshein, Luca Antiga, Alban Desmaison, Andreas Kopf, Edward Yang, Zachary DeVito, Martin Raison, Alykhan Tejani, Sasank Chilamkurthy, Benoit Steiner, Lu Fang, Junjie Bai, and Soumith Chintala. Pytorch: An imperative style, high-performance deep learning library. In H. Wallach, H. Larochelle, A. Beygelzimer, F. d'Alché-Buc, E. Fox, and R. Garnett, editors, *Advances in Neural Information Processing Systems 32*, pages 8024–8035. Curran Associates, Inc., 2019.

[82] Gunnar A Sigurdsson, Gül Varol, Xiaolong Wang, Ali Farhadi, Ivan Laptev, and Abhinav Gupta. Hollywood in homes: Crowdsourcing data collection for activity understanding. In *European Conference on Computer Vision*, pages 510–526. Springer, 2016.

[83] Diederik P Kingma and Jimmy Ba. Adam: A method for stochastic optimization. *arXiv preprint arXiv:1412.6980*, 2014.

[84] Ho Kei Cheng, Yu-Wing Tai, and Chi-Keung Tang. Rethinking space-time networks with improved memory coverage for efficient video object segmentation. In *Advances in Neural Information Processing Systems*, 2021.

[85] Vicky Kalogeiton, Philippe Weinzaepfel, Vittorio Ferrari, and Cordelia Schmid. Action tubelet detector for spatio-temporal action localization. In *Proceedings of the IEEE International Conference on Computer Vision*, pages 4405–4413, 2017.

[86] Akash Kumar and Yogesh Singh Rawat. End-to-end semi-supervised learning for video action detection. In *Proceedings of the IEEE/CVF Conference on Computer Vision and Pattern Recognition*, pages 14700–14710, 2022.

[87] Yubo Zhang, Pavel Tokmakov, Martial Hebert, and Cordelia Schmid. A structured model for action detection. In *Proceedings of the IEEE/CVF Conference on Computer Vision and Pattern Recognition*, pages 9975–9984, 2019.

[88] Jiajun Tang, Jin Xia, Xinzhi Mu, Bo Pang, and Cewu Lu. Asynchronous interaction aggregation for action detection. In *European Conference on Computer Vision*, pages 71–87. Springer, 2020.

[89] Yu-Lun Liu, Yi-Tung Liao, Yen-Yu Lin, and Yung-Yu Chuang. Deep video frame interpolation using cyclic frame generation. In *Proceedings of the AAAI Conference on Artificial Intelligence*, volume 33, pages 8794–8802, 2019.

Checklist

1. For all authors...
   (a) Do the main claims made in the abstract and introduction accurately reflect the paper's contributions and scope? [Yes]
   (b) Did you describe the limitations of your work? [Yes]
   (c) Did you discuss any potential negative societal impacts of your work? [Yes] Discussed in the supplementary material
   (d) Have you read the ethics review guidelines and ensured that your paper conforms to them? [Yes]
2. If you are including theoretical results...
   (a) Did you state the full set of assumptions of all theoretical results? [N/A]
   (b) Did you include complete proofs of all theoretical results? [N/A]
3. If you ran experiments...
   (a) Did you include the code, data, and instructions needed to reproduce the main experimental results (either in the supplemental material or as a URL)? [Yes]
   (b) Did you specify all the training details (e.g., data splits, hyperparameters, how they were chosen)? [Yes]
   (c) Did you report error bars (e.g., with respect to the random seed after running experiments multiple times)? [No]
   (d) Did you include the total amount of compute and the type of resources used (e.g., type of GPUs, internal cluster, or cloud provider)? [Yes] Detailed in supplementary
4. If you are using existing assets (e.g., code, data, models) or curating/releasing new assets...
   (a) If your work uses existing assets, did you cite the creators? [Yes]
   (b) Did you mention the license of the assets? [N/A]
   (c) Did you include any new assets either in the supplemental material or as a URL? [No]
   (d) Did you discuss whether and how consent was obtained from people whose data you're using/curating? [N/A] Public data used.
   (e) Did you discuss whether the data you are using/curating contains personally identifiable information or offensive content? [N/A]
5. If you used crowdsourcing or conducted research with human subjects...
   (a) Did you include the full text of instructions given to participants and screenshots, if applicable? [N/A]
   (b) Did you describe any potential participant risks, with links to Institutional Review Board (IRB) approvals, if applicable? [N/A]
   (c) Did you include the estimated hourly wage paid to participants and the total amount spent on participant compensation? [N/A]

A Appendix

We present additional analysis, experiments and details for various components in the main manuscript. We perform detailed ablations on different loss function and analysis of using varying σ for the proposed *MGW-Loss*, which provides detailed explanation for effect of σ on performance and validates our choice of σ for all experiments in the main paper. We also explain the potential social impact our work can have (positive and negative) in detail.

B Potential Social Impact

This work can have positive and negative impact on future learning task related to complex video understanding by reducing the amount of annotations needed for training a model. On the positive side, while the iterative selection can take longer initially, it will save multiple hours on annotation for a large scale dataset. A negative impact of this approach is its use to select and annotate data for surveillance and intrusive monitoring. However, this can improve general video understanding at large since the cost of annotating large dataset will be significantly less with this approach.

C Loss function details

The proposed *MGW-Loss* formulation is able to handle sparse annotations via interpolation of known ground truth annotations and a Gaussian based weight estimation. Interpolation gives the in-between annotation frames for a clip with sparse ground truth annotation, which allows the use of traditional loss computation directly. However, since interpolation can be of low quality and not necessarily on the correct region of frame, using it as is affects the network's learning process due to adverse noise. While we could directly mask frames with ground truth annotation and only use those for loss computation, it is not able to train a model with low loss for initial frame selection algorithm. Table 5 and 6 shows the performance gap for model trained with different loss types (masking, interpolation and *MGW* loss). To utilize the ground truth annotated frames fully while giving only partial importance to the interpolated frames, we propose our *Max-Gaussian Weighted Loss* which uses a Gaussian distribution to give weight to the neighboring interpolated annotations. The Gaussian is fixed around each ground truth annotation and the value for each frame is used as its weight during loss computation. So an annotated frame further away from actual ground truth will have very low weight compared to one near to the actual ground truth. Figure 8 visually demonstrates the annotations for loss computation using masking, interpolation and proposed Gaussian interpolation variation in the *MGW-Loss* function. We also show that the Gaussian weighted interpolation gives best performance in table 5 and 6.

Table 5: Comparison between different loss functions in UCF-101 for different percent of annotated frames per video. For each setting, we train the model using the masking loss, the interpolation loss and the proposed *MGW* loss with $\sigma = 1.3$.

Annotation Percent	Loss Type	**v-mAP@**				**f-mAP@**			
		0.1	0.2	0.3	0.5	0.1	0.2	0.3	0.5
1%	Masking	97.89	93.45	86.53	59.4	91.04	88.25	83.54	60.10
1%	Interpolation	97.99	94.24	87.69	63.71	91.14	88.45	83.69	64.04
1%	MGW	98.07	95.37	89.01	63.94	91.28	88.41	83.85	64.69
5%	Masking	98.01	95.10	89.98	67.60	93.18	90.07	87.78	66.50
5%	Interpolation	98.05	95.30	90.28	69.41	93.21	91.30	88.16	68.41
5%	MGW	98.12	96.01	90.95	71.89	93.38	91.28	88.71	70.91
10%	Masking	98.1	95.84	90.23	69.90	94.02	92.05	88.30	69.30
10%	Interpolation	98.18	96.43	91.12	71.52	94.07	92.07	88.10	70.57
10%	MGW	98.14	96.46	91.12	73.20	94.05	92.03	88.72	71.75

C.1 Selection of sigma (σ)

To further illustrate the effects of varying values of sigma (σ) in the proposed *MGW-Loss* function, we evaluate the same loss function at different sigmas in table 7. We show different weight distributions

Table 6: Comparison between different loss functions in JHMDB for different percent of annotated frames per video. For each setting, we train the model using the masking loss, the interpolation loss and the proposed *MGW* loss with $\sigma = 1.3$.

Annotation Percent	Loss Type	v-mAP@				f-mAP@			
		0.1	0.2	0.3	0.5	0.1	0.2	0.3	0.5
3%	Masking	98.01	96.18	90.26	57.81	95.10	92.39	86.84	59.74
3%	Interpolation	98.80	96.70	95.03	65.47	95.40	93.55	89.02	68.48
3%	MGW	98.80	96.77	95.15	65.56	95.38	93.54	89.94	68.78
6%	Masking	98.71	96.25	91.04	63.78	95.26	92.32	88.26	67.53
6%	Interpolation	98.89	97.98	95.09	68.41	97.10	95.80	92.85	71.48
6%	MGW	98.90	97.94	95.20	70.75	97.09	95.78	93.09	74.09
9%	Masking	99.10	98.01	93.18	69.22	95.91	93.96	90.17	69.81
9%	Interpolation	99.22	98.35	95.42	72.35	96.30	94.51	92.48	72.57
9%	MGW	99.18	98.41	95.58	74.01	96.32	94.53	92.67	74.49

for various sigma values in figure 9, with the loss behaving as masking loss at very low sigma ($\sigma < 0.01$) and as interpolation loss at high sigma ($\sigma > 5$). Since *MGW-Loss* will consider weights for the interpolation based pseudo-labeled neighboring frames based on their distance from the annotated frame, the value of σ will affect it significantly. Low sigma will give little to no weight to neighbor frames while very high sigma will give all pseudo-labeled frames equal weights, which might be incorrect with sparse annotations. Based on this, we prefer to pick a moderate sigma value that gives partial weight to neighboring frames. We conduct our experiments with sigma values of $\sigma = 1.3$ and $\sigma = 2.5$ in table 7. It is found that a leaner distribution using $\sigma = 1.3$ gives better initialization with sparse frames than $\sigma = 2.5$ since interpolated annotations are not as trustworthy in the beginning. Due to a stronger initialization, $\sigma = 1.3$ stays ahead and gives best scores for higher annotation percentages as well.

Table 7: Results of using various values for σ in the proposed *MGW-Loss* in UCF-101. The effect of *MGW-Loss* changes for different values of σ, with it behaving as masking loss at $\sigma = 0$, interpolation loss at $\sigma >= 5$ and *MGW* loss at $0 < \sigma < 5$.

Annotation Percent	Sigma σ	v-mAP@				f-mAP@			
		0.1	0.2	0.3	0.5	0.1	0.2	0.3	0.5
1%	0	97.89	93.45	86.53	59.4	91.04	88.25	83.54	60.1
1%	1.3	98.07	95.37	89.01	63.94	91.28	88.41	83.85	64.69
1%	2.5	98.01	95.17	89.00	63.79	91.20	88.35	83.69	64.38
1%	5	97.99	94.24	87.69	63.71	91.14	88.45	83.69	64.04
5%	0	98.01	95.1	89.98	67.6	93.18	90.07	87.78	66.50
5%	1.3	98.12	96.01	90.95	71.89	93.38	91.28	88.71	70.91
5%	2.5	98.1	95.89	90.78	71.55	93.3	91.25	88.56	70.26
5%	5	98.05	95.3	90.28	69.41	93.21	91.3	88.16	68.41
10%	0	98.10	95.84	90.23	69.9	94.02	92.05	88.30	69.30
10%	1.3	98.14	96.46	91.12	73.2	94.05	92.03	88.72	71.75
10%	2.5	98.10	96.45	91.11	73.07	94.05	92.02	88.68	71.59
10%	5	98.18	96.43	91.12	71.52	94.07	92.07	88.10	70.57

C.2 Influence of Lambda λ

We perform an experiment to study the influence of λ on Eq. 3. The effect of different values of λ is shown in table 8. We observe that giving higher weight to uncertainty (λ = 0.75) reduces overall score as it ignores proximity value. Having lower weight on uncertainty (λ = 0.25) on the other hand promotes more distance and performs better than λ = 0.75. Although λ = 0.25 has higher f-mAP @ 0.5, we do not optimize this hyperparameter and use equal weight in the paper (λ = 0.5).

C.3 Influence of Tau τ in non-activity suppression

As the model is very certain on most background pixels early on in the training, we observed that this gives us a large margin between the true background pixel confidence value and the uncertain pixel

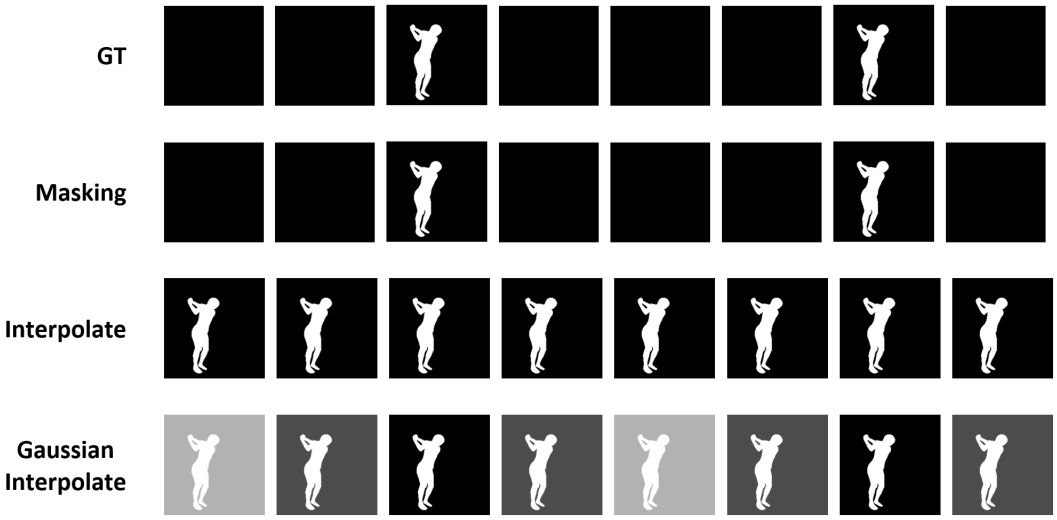

Figure 8: Representation of using different σ values for *MGW-Loss* computation. **Row 1:** Ground truth annotation (sparse) for a single video clip. **Row 2:** *MGW* with $\sigma = 0$ (equivalent to masking out frames with GT present for loss computation). **Row 3:** *MGW* with high σ (High weight given to all neighboring frames, equivalent to using interpolated ground truth annotations). **Row 4:** *MGW* with $\sigma = 1.3$ (Max Gaussian value used as weight for each interpolated annotation).

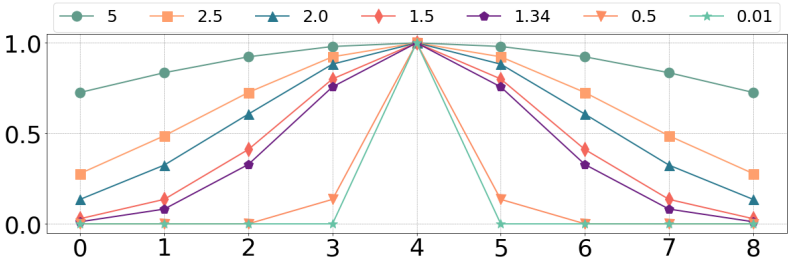

Figure 9: Weight distribution for different values of sigma σ for the *MGW-Loss* function. Horizontal axis shows the frames for a sample clip (with ground truth annotation at frame 4) and vertical axis shows the weights given to each frame based on *MGW-Loss* with varying σ. The weights for σ from 0.01 till 5 is shown here, with $\sigma < 0.01$ acting as masking loss and $\sigma > 5$ acting as interpolation loss and the values in between representing *MGW* loss.

Table 8: Influence of λ and τ in the training. We evaluate the effect of using different value of λ and τ on UCF-101 using the proposed *APU* to increase annotations from 5% to 10%.

Lambda	**v-mAP@**		**f-mAP@**		Tau	**v-mAP@**		**f-mAP@**	
(λ)	0.3	0.5	0.3	0.5	(τ)	0.3	0.5	0.3	0.5
0.5	91.12	73.20	88.72	71.75	0.3	90.96	72.42	88.24	71.65
0.25	92.34	72.59	88.65	71.83	0.4	91.12	73.20	88.72	71.75
0.75	90.99	72.09	88.06	71.67	0.5	91.24	73.15	88.55	71.77

confidence value. We perform ablation with different τ values and show them in table 8. We observe that changing τ affects the results slightly and hyperparameter tuning can affect the final results with small margin. We did not perform hyperparameter tuning for τ in our proposed method.

D Comparison to prior supervised approach

We compare our proposed approach with prior supervised methods in Table 9 on UCF-101 and J-HMDB dataset. Using only 10% of annotation on both datasets, our *APU+MGW-Loss* based

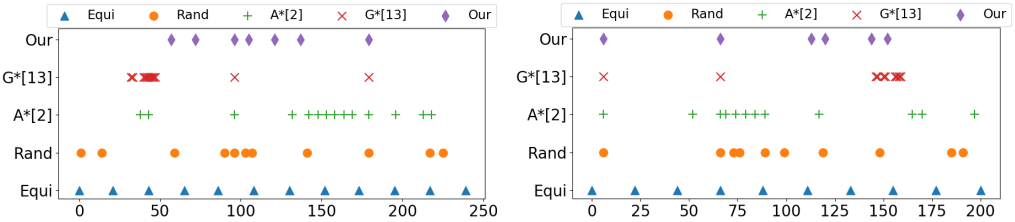

Figure 10: Visualization of frames selected using different cost functions for **(Left)** Soccer Juggling, **(Right)** Dog Walking. We show results for Our, random, equidistant, G*: Gal et al. [73] and A*: Aghdam et al. [53], with all methods using same detection backbone for fair comparison. We visualize two videos with long continuous actions, where our global ranking based frame selection approach selects only few frames for annotation which are well spaced. Both baseline active learning methods (G*, A*) end up selecting more frames since they don't have global ranking in their formulation. Non-active learning baseline (random, equidistant) select frames without any utility information. Our method has better cost utilization by reducing redundant samples while maintaining better performance than any other baseline method.

approach performs comparably with the same backbone using 100% annotation. Our 10% model's f-mAP@0.5 and v-mAP@0.5 is closer to multiple prior supervised models and can be trained with a simpler end-to-end method.

Table 9: Comparison with prior state-of-the-art supervised methods on UCF-101 and J-HMDB. We evaluate our full approach on v-mAP and f-mAP scores using only 10% annotation data. **f@** denotes **f-mAP@**. † is trained in weakly-supervised manner.

Method	Annot Percent	UCF-101					J-HMDB				
		f@	**v-mAP@**				**f@**	**v-mAP@**			
		0.5	0.1	0.2	0.3	0.5	0.5	0.1	0.2	0.3	0.5
Peng et al. [7]	100%	65.7	77.3	72.9	65.7	35.9	58.5	-	74.3	-	73.1
TCNN [8]	100%	67.3	77.9	73.1	69.4	-	61.3	-	78.4	-	-
Gu et al. [78]	100%	76.3	-	-	-	59.9	73.3	-	-	-	-
ACT [85]	100%	69.5	-	76.5	-	-	-	-	74.2	-	73.7
STEP [10]	100%	75.0	83.1	76.6	-	-	-	-	-	-	-
Rel. Graph [87]	100%	77.9	-	-	-	-	-	-	-	-	-
AIA [88]	100%	78.8	-	-	-	-	-	-	-	-	-
VidsCapsNet [9]	100%	78.6	98.6	97.1	93.7	80.3	64.6	98.4	95.1	89.1	61.9
Ours	100%	74.0	98.3	96.9	91.5	75.2	74.9	99.2	99.2	96.4	75.8
Ours †	10%	71.7	98.1	96.5	91.1	73.2	74.5	99.2	98.4	95.6	74.0

E Frame selection details

E.1 Uncertainty using dropout

We follow [73] to use dropout for generating uncertainty during inference. We apply *3D Dropout* with a dropout probability of 0.5 before the final convolution layer in the decoder network from [9]. This dropout layer is enabled during inference, enabling uncertainty in the output by avoiding memorization. We pass the same clip 10 times in the network with dropout enabled and collect the output for uncertainty based scoring for each frame.

E.2 Selection step size

Another crucial factor that can affect learning process initially is the frame selection step size. This is directly related to the time needed for training. Larger step size will take shorter time as fewer selection iterations are needed to expand the dataset while shorter step size will need multiple selection iterations and can take longer as a result. Table 10 shows the difference of slow increment vs fast increment vs random selection. While doing a larger step size of 5%, our final result is already significantly better than random selection. When we perform annotation improvement for smaller

Table 10: Comparison between frame selection with different step size in UCF-101. For each setting, we use the *MGW-Loss* with $\sigma = 1.3$ for consistency. We use the the proposed **APU** frame selection method. We start with an initial random seed annotation and increase annotations by given step size in each iteration.

Annotation	**v-mAP@**				**f-mAP@**			
Percent	0.1	0.2	0.3	0.5	0.1	0.2	0.3	0.5
Step size 1%								
1%	98.07	95.37	89.01	63.94	91.28	88.41	83.85	64.69
2%	98.07	95.41	89.42	66.4	92.14	88.65	84.20	67.10
3%	98.08	95.68	90.01	69.52	93.84	89.05	86.11	69.02
4%	98.12	95.89	90.72	71.00	94.04	89.89	87.51	70.00
5%	98.12	96.10	91.03	72.20	94.10	91.35	88.62	70.99
6%	98.15	96.18	91.03	72.70	94.12	91.52	88.73	71.31
7%	98.14	96.27	91.12	73.05	94.10	91.68	88.85	71.55
8%	98.15	96.32	91.15	73.21	94.14	91.84	88.80	72.47
9%	98.19	96.45	91.22	73.82	94.15	92.10	88.84	72.76
10%	98.22	96.58	91.22	73.94	94.15	92.10	88.89	72.91
Step size 5%								
1%	98.07	95.37	89.01	63.94	91.28	88.41	83.85	64.69
5%	98.12	96.01	90.95	71.89	93.38	91.28	88.71	70.91
10%	98.14	96.46	91.12	73.20	94.05	92.03	88.72	71.75

Table 11: Comparison between different frame selection method (Global selection vs Local selection) in JHMDB. For each setting, we train the model using the *MGW-Loss* with $\sigma = 1.3$.

Annotation	**v-mAP@**				**f-mAP@**			
Percent	0.1	0.2	0.3	0.5	0.1	0.2	0.3	0.5
Global								
3%	98.81	96.77	95.15	65.56	95.38	93.54	89.94	68.78
6%	98.97	97.94	95.2	70.75	97.09	95.78	93.09	74.09
9%	99.18	98.41	95.58	74.01	96.32	94.53	92.67	74.50
Local								
3%	98.81	96.77	95.15	65.56	95.38	93.54	89.94	68.78
6%	98.82	97.12	95.18	69.44	96.21	94.04	91.87	72.81
9%	99.15	98.08	95.19	72.83	96.25	94.73	92.48	73.55

step size of 1%, we notice that the performance is consistently better than larger step size. With a slow step size, our 10% data variant significantly outperforms both 10% with large step size and 10% random frame selection.

E.3 Local vs Global frame selection

Frame selection can be done locally per each video or globally across all videos. While local frame selection will select top K% frames with highest utility score for a given video, it might not take into account similar frames across other videos for same class. This poses a possibility for redundant information in the annotation. Since our goal is to reduce annotation budget while increasing information for fewest annotations possible, we want to utilize our annotation budget wisely. A possible solution is to globally rank the frames based on utility across all videos, while still maintaining distance based scoring. We propose the global frame selection process, where we score the frames for each video based on Gaussian distance from closest annotated frame in that video, but rank them globally across all videos. Once a frame is selected, we update the score for all other frames nearby based on distance and re-rank them. The score updating is only done for distance based factors of the equation and does not need running of the frames through the model again, reducing any significant extra time compared to local frame selection. Table 11 shows the difference between doing local selection vs global selection, where the network learns better from annotations curated using the global selection method. We further evaluate the per class score for frame selection method in table 12. We can see the difference in number of frames selected for each class in global and local method, which shows that global selection prioritizes frame selection over

Table 12: Per class score for Global vs Local frame selection method on JHMDB dataset. We report the number of frames selected and the score for video level AP and frame level AP at IoU @ 0.5 for global selection method and local selection method.

Class	**Frame selection**		**Global scores**		**Local scores**	
	Global	Local	video-AP	frame-AP	video-AP	frame-AP
brush_hair	391	232	0.75	0.68	0.67	0.60
catch	155	272	0.21	0.14	0.00	0.06
clap	382	248	1.00	0.90	0.85	0.86
climb_stairs	123	224	0.00	0.00	0.00	0.06
golf	240	240	0.00	0.10	0.00	0.05
jump	68	216	0.08	0.14	0.08	0.12
kick_ball	72	200	0.00	0.00	0.00	0.00
pick	110	224	0.08	0.22	0.33	0.24
pour	404	312	0.94	0.89	1.00	0.87
pullup	405	312	0.19	0.20	0.13	0.22
push	108	240	0.17	0.22	0.08	0.15
run	89	232	0.27	0.27	0.27	0.25
shoot_ball	133	232	0.00	0.02	0.00	0.01
shoot_bow	458	304	1.00	0.72	1.00	0.89
shoot_gun	343	312	0.25	0.30	0.25	0.19
sit	284	216	0.58	0.53	0.58	0.52
stand	254	200	0.64	0.65	0.64	0.68
swing_baseball	332	312	0.00	0.05	0.00	0.17
throw	430	280	0.27	0.17	0.18	0.15
walk	166	232	0.17	0.14	0.17	0.18
wave	333	240	0.92	0.93	0.67	0.66

Table 13: Comparison between the proposed frame selection method and sample selection method in UCF-101. Sample selection method selects entire video for annotation at the given percentage.

Annotation	**v-mAP@**				**f-mAP@**			
Percent	0.1	0.2	0.3	0.5	0.1	0.2	0.3	0.5
Our (Frame)								
1%	98.07	95.37	89.01	63.94	91.28	88.41	83.85	64.69
5%	98.12	96.01	90.95	71.89	93.38	91.28	88.71	70.91
10%	98.14	96.46	91.12	73.20	94.05	92.03	88.72	71.75
Sample								
1%	89.48	76.81	61.02	23.42	76.47	69.37	58.64	31.65
5%	91.81	82.88	70.85	36.24	81.41	75.02	66.43	42.68
10%	95.94	88.89	79.35	48.21	86.71	81.33	73.87	50.37

certain classes while local selection tries to pick same number of sample for each of the video. We observe that for most classes which global selection picks more frames from are scoring higher than the local selection counterpart.

E.4 Frame vs Sample selection

We evaluate the alternate sampling technique in which we start with only a fraction of videos fully annotated and select the videos to annotate in each active learning step. This is different to our frame selection strategy where we assume all videos have a fraction of frames annotated and we only select which frames to annotate from all videos in each active learning step. Sample selection is a more costly approach as each selected video has to be fully annotated for all frames, which adds annotation cost for little gain in knowledge. We show the results for UCF-101 and JHMDB dataset in table 13 and 14 respectively for sample selection vs our frame selection method.

Table 14: Comparison between the proposed frame selection method and sample selection method in JHMDB. Sample selection method selects entire video for annotation at the given percentage.

Annotation Percent	v-mAP@ 0.1	0.2	0.3	0.5	f-mAP@ 0.1	0.2	0.3	0.5
Our (Frame)								
3%	98.81	96.77	95.15	65.56	95.38	93.54	89.94	68.78
6%	98.97	97.94	95.2	70.75	97.09	95.78	93.09	74.09
9%	99.18	98.41	95.58	74.01	96.32	94.53	92.67	74.50
Sample								
3%	87.36	86.94	81.05	47.42	87.98	86.22	80.11	50.09
6%	92.05	90.45	88.24	53.69	90.36	89.74	85.88	56.32
9%	94.15	92.18	90.76	57.33	93.68	91.85	90.30	58.85

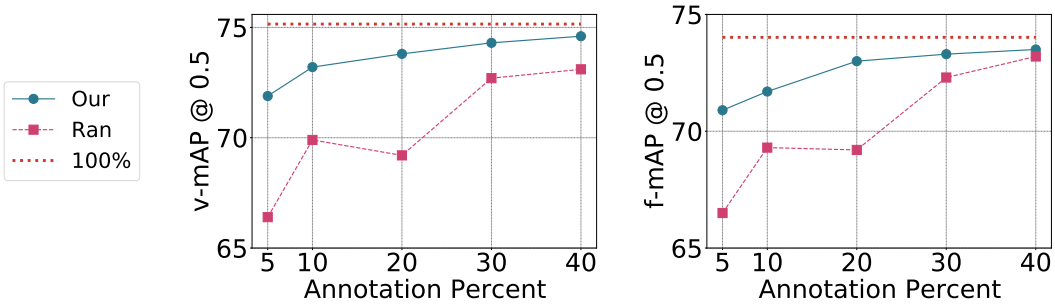

Figure 11: Extending random baseline and our *APU* approach till convergence for UCF-101 (v-mAP, f-mAP @ 0.5 IoU).

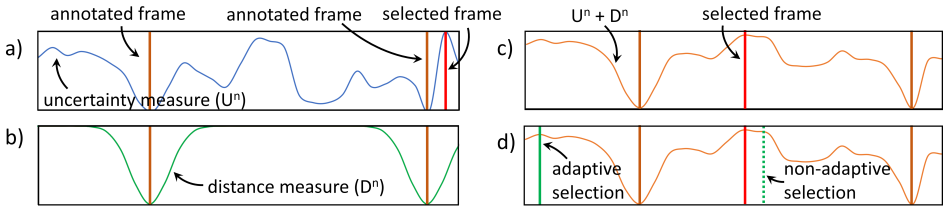

Figure 12: Active frame selection using APU scoring function. a) frame selection based on just uncertainty, b) showing distance measure based on existing annotations, c) frame selection using proposed APU scoring function, and d) difference between frame selection with adaptive and non-adaptive scoring.

E.5 Extending annotation to convergence

We extend the baselines as well as our method further in Figure 11, where we see that the baselines eventually converge close to fully-supervised scores with additional annotations. Our *APU* frame selection approach gets higher score earlier and saturates from 20% annotation while the random baseline catches up at around 40% annotation, demonstrating *APU*'s need for less annotation to achieve higher scores.

E.6 Cost function variations

Frame selection can be done through different scoring mechanisms such as random selection, uncertainty based selection or our *Adaptive Proximity-aware Uncertainty (APU)* based selection. Each selection method gives different set of frames for further annotation to the oracle. Our goal is to select frames with maximum utility for further annotation such that the network can learn better from it. Random frame selection works as the baseline method, where frames are selected at random for annotation. We compare that against uncertainty based selection method, where each frame is scored

Algorithm 1 Active Sparse Learning (ASL) algorithm

Input: videos $\mathcal{V}$; total budget b; labelled frames F_L; number of trails T; pixels per frame I^p; current model $\mathcal{M}^c$; frame annotation cost C_{frame}

Initialize: budget b_s = 0; frames to annotate $F_{annot} \leftarrow \{\}$

for all videos v in $\mathcal{V}$ **do**
  for all frame i in $f_{v,u}$ **do** *// Iterate over each unannotated frame*
    $Uncertainty(U^i) = U(\mathcal{M}^c, i)$ *// Compute uncertainty of frame i with Eq. 1*
while $b_s \leq b$ **do**
  APU_score $\leftarrow \{\}$ *// Initialize empty list to store all frame's APU score*
  for all videos v in $\mathcal{V}$ **do**
    for all frame i in $f_{v,u}$ **do** *// Iterate over each unannotated frame*
      D^i = $D(f_{v,l}, i)$ *// Compute distance score of frame i using Eq. 2*
      $\mathcal{U}^i_{APU} = (U^i, D^i)$ *// Compute frame i utility score using Eq. 3*
      Append $\mathcal{U}^i_{APU}$ to APU_score
  $f_{max} \leftarrow$ max(APU_score) *// Get frame with highest utility*
  Append f_{max} to F_{annot} *// Add highest utility frame for annotation*
  $F_L \leftarrow F_L \cup f_{max}$ *// Mark frame as annotated for future distance scores*
  $b_s \leftarrow b_s + C_{frame}$ *// Increment cost for each frame added to annotation*
return F_L, F_{annot} *// Return new labelled frames and set for annotation*

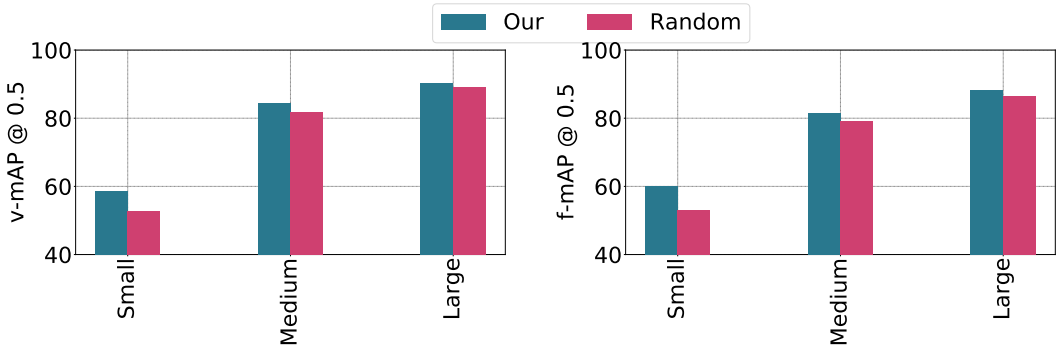

Figure 13: Evaluation of performance of the model with respect to relative area of the spatio-temporal annotation.

based on the uncertainty score as [73]. While this method highlights regions that are more uncertain and need extra annotation, it fails to take into account the temporal factor for the scoring process and ends up selecting frames from similar region. Our *APU* based method adapts to each new annotation and scores nearby frames lower, thus encouraging frame selection from different regions. Figure 12 demonstrates how the proposed *APU* selection method picks optimum frames compared to other techniques. We compare sample selection using *APU* and other baseline methods in figure 10. Unlike uncertainty based method, our *APU* based selection method selects frames further from each other and allows more variation in annotation.

E.7 Selection algorithm

We describe our selection algorithm from the main manuscipt in algorithm 1. Once we have a model trained ($\mathcal{M}^c$), we iterate over each video and get the uncertainty score for each unannotated frame. This step requires the model output so we run it once for all the videos for each active learning cycle. Then we need to compute the distance score for each frame, combine it with the uncertainty score for that frame and then pick the frame among all videos with the highest utility. Since the distance score computation has to be recomputed for each video which had a new annotation frame added, we also recompute the total utility score for those videos. However, as the uncertainty score does not need to be recomputed, this process is fairly fast. We keep on adding frame for annotation until we exhaust the budget for that active learning round. At the end we return a set of frames selected based on their utility for the oracle to annotate and add to labeled set.

E.8 Performance based on annotation area

Similar to MS-COCO dataset, we also separated the evaluation set into small, medium and large based on each video's average activity area with respect to the frame size [Small < 702, Medium >= 702 and < 1302, Large >= 1302 in square pixels for UCF-101]. With this distinction, we had 267 small videos, 479 medium videos and 164 large videos. As all video classes don't have all three variations, some of the classes don't exist in small and large sets. As such, we only compare the common classes across all three sets for equivalent comparison. From Figure 13, we see that our approach selects samples to improve small and medium sized actions more compared to random selection baseline

F VOS task

We demonstrate the effectiveness of our approach on video object segmentation task using [84] and [77] networks. We show the results for [77] network in table 15, where we compare with baseline active learning methods using random, uncertainty-based [73], entropy-based [53] with our proposed active learning method. We observe that the overall score in each incremental step is higher for the frames selected by our active learning method compared to all baselines, further validating the generalization of our approach on different video understanding task.

Table 15: Comparison of the proposed method on YouTube-VOS 2019 dataset with baseline active learning methods using LSTM based VOS network from [77]. *R* = Random, *A* = Aghdam et al. [53], *G* = Gal et al. [73]. * is extended to video object segmentation using same segmentation network as [77].

	Overall			$\mathcal{J}_S$			$\mathcal{J}_U$			$\mathcal{F}_S$			$\mathcal{F}_U$		
Method	10%	20%	30%	10%	20%	30%	10%	20%	30%	10%	20%	30%	10%	20%	30%
Random	20.9	24.5	26.3	26.6	30.2	33.4	20.1	23.4	24.5	19.8	24.1	25.9	17.0	20.5	21.4
A *[53]	22.7	26.7	34.8	30.4	34.2	41.8	20.3	23.2	30.0	22.8	28.4	39.7	17.6	21.1	27.6
G * [73]	21.7	26.0	33.3	30.2	30.4	41.2	19.7	20.3	30.2	21.0	22.8	34.4	15.9	17.6	27.3
Our	24.3	33.3	38.1	31.5	41.2	45.7	22.5	30.2	32.1	24.0	34.4	42.9	19.3	27.3	31.6

G Network implementation details

G.1 Action detection network

We use the 2D variant of video capsule network [9] for action detection task on UCF-101-24 and JHMDB-21 dataset. The network takes an input clip of $T \times H \times W \times C$ dimension [T=frames, H=height, W=width, C=channels] and outputs T frames of $H \times W \times 1$ dimension. It also predicts the class prediction vector for the entire clip. The 2D capsule network takes a batch size of 8 samples per iteration, with each sample clip of size $8 \times 224 \times 224 \times 3$ with a temporal skip rate of 2. We follow the same input/output format as the original paper for 3D capsule network [9] for the 2D network variant. The full architecture detail is shown in figure 14.

G.2 VOS network

We use our technique on two separate newtorks for the video object segmentation task. We use the method by [84] that recently had state-of-the-art performance on YouTube-VOS 2019 challenge. This network takes an input clip of 3 frames and learns up-to 2 objects segmentation across those 3 frames in training time. We also test our method in a simpler network used for VOS task based on ConvLSTM modules [77]. It takes as input a clip of T frames of $H \times W \times C$ dimension and the annotation mask of first frames of the clip of size $H \times W \times 1$. The network outputs predicted segmentation mask of size $T \times H \times W \times C_{class}$. For both networks we use clips with frames of size $224 \times 224 \times 3$ and annotation of size $224 \times 224 \times 1$ as input and the networks output segmentation clip with size $224 \times 224 \times 1$. The first method [84] takes 3 frames input in the clip while the second method [77] takes 32 frames input in the clip. The object of interest annotated in the first frame will be segmented through the clip. During inference, we use the annotation of the last frame predicted as the input annotation mask for the next subsequent clip. We use a batch size of 8 for this task as well.

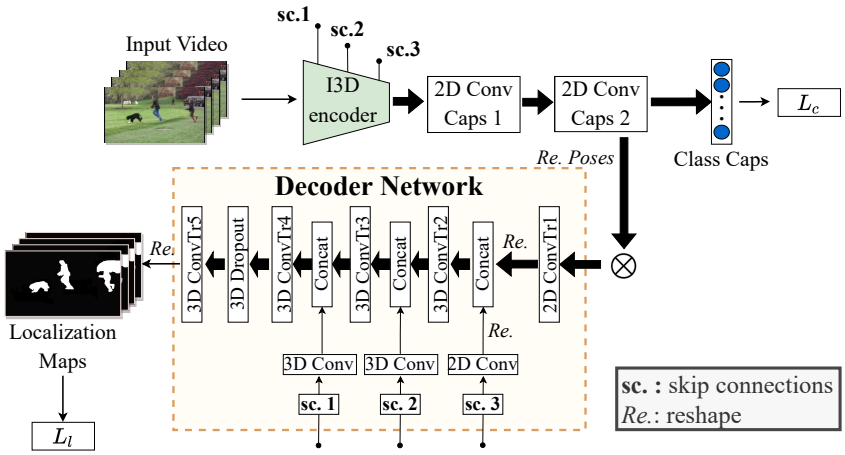

Figure 14: Overview of the proposed action detection network. Based on [9], features are extracted from input frames using I3D [15] architecture based encoder. We take features from $Mixed_4f$ layer of I3D network. This is then followed by two $2D\ convolutional\ capsule$ layers which outputs class capsules. The class capsules is used for final class prediction and classification loss computation. This is followed by series of transpose convolution layers (2D and 3D) for upscaling the feature map and concatenation with features from intermediate layers of the I3D encoder via skip connections. We finally obtain the localization maps of same size as input video, which is used for detection loss.

Table 16: Comparison between Kinetics pre-trained and Charades pre-trained weights for UCF-101 dataset. We show the f-mAP and v-mAP scores at 0.5 IoU for different annotation size.

	f-mAP @ 0.5			v-mAP @ 0.5		
Pre-train	1%	5%	10%	1%	5%	10%
Charades	60.7	66.5	69.3	59.2	66.4	69.9
Kinetics	60.4	66.5	69.0	59.2	66.2	69.8

G.3 Technical details

We train our model using a single *16GB Nvidia RTX 5000 GPU* with Turing architecture. The frame selection method only runs in inference mode with *Dropout* enabled, thus using only a fraction of the GPU memory. Due to this, we can run multiple instances in parallel for frame selection in the training video set, reducing the time taken for frame selection process. During each iteration, we only select the given percentage of frames for further annotation and we retain the previous set of annotated frames. On a 8 core 3.2 GhZ Intel CPU and 16GB Nvidia RTX 5000 GPU combination the frame selection round takes **50 minutes** for UCF-101 (432K training frames). We run a total of 2 active learning cycles for frame selection in the main experiments (1% -> 5% and 5% -> 10%). The model training for UCF-101 takes about **15 minutes** per epoch, which is trained for 40 epochs for each set of annotations.

G.4 Interpolation:

The annotation interpolation for UCF-101 is done using linear interpolation of the bounding box corners. The pixel-wise annotation interpolation for J-HMDB is done using CyclicGen [89]. In case of edge frames or single frame annotations, we extrapolate the annotation to other frames.

G.5 Pre-trained weights:

While we follow prior works and use Charades pre-trained weights in our experiments, we also compare with Kinetics-400 pre-trained weights in table 16. This shows that the pre-trained weights selection will not affect the trend from *APU* selection.